TÜBİTAK

Turkish Journal of Physics

http://journals.tubitak.gov.tr/physics/

Research Article

Turk J Phys
(2014) 38: 563 – 572
© TÜBİTAK
doi:10.3906/fiz-1407-9

Nanosphere lithography – exploiting self-assembly on the nanoscale for sophisticated nanostructure fabrication

Eser Metin AKINOGLU[1], **Anthony John MORFA**[1,*], **Michael GIERSIG**[1,2,*]
[1]Department of Physics, Freie Universität Berlin, Berlin, Germany
[2]Department of Chemistry, Adam Mickiewicz University, Poznan, Poland

Received: 09.07.2014 • **Accepted:** 01.10.2014 • **Published Online:** 10.11.2014 • **Printed:** 28.11.2014

Abstract: We demonstrate the fabrication of sophisticated nanostructures using nanosphere lithography (NSL). These include periodic triangular and pyramidal islands as well as periodically perforated thin films and cavities on the nano- and microscale. Furthermore, periodic arrays of vertically standing multiwalled carbon nanotubes are grown by plasma enhanced chemical vapor deposition from catalyst islands that were prepatterned by NSL. Moreover, we discuss the applicability of NSL to rough surfaces and show that the ratio between nanosphere size and roughness is determinant of the resulting nanostructure produced. Excellent, limited, and bad applicability of NSL are shown for smooth, rough, and very rough surfaces, respectively. Finally, we demonstrate that NSL is applicable to orthopedic implants. The results of this work will facilitate the fabrication of different nanostructured surfaces with well-defined morphologies and properties towards the customized rational design of medically relevant surfaces.

Key words: Nanosphere lithography, nanofabrication, nanostructured surface, self-assembly, multiwalled carbon nanotubes

1. Introduction

Naturally occurring functional surfaces such as the water-repellent and self-cleaning surfaces of some plant species, commonly termed the lotus leaf effect, are observed throughout nature. Through advances in microscopic, spectroscopic, and fabrication methods of nanoscale materials, a better understanding and so-called biomimetic reproduction of such functional surfaces has been possible in the past several decades. Two common examples whereby the properties of functional biosurfaces have been studied and ultimately ascribed to structures with morphologies on the micro- and nanoscale include water-repellent plant surfaces observed on *Nelumbo nucifera*, commonly referred to as the lotus leaf effect, as well as the antifogging eyes of *C. pipiens* [1,2]. Today, many different chemical and physical top-down methods, i.e. by removing material from bulk materials ultimately forming nanostructures, as well as bottom-up methods, i.e. assembling nanostructures from smaller units, are known for the fabrication of nanoscale materials [3,4]. The control over size, shape, and morphology of nanostructures can be achieved using different lithographic techniques such as extreme ultraviolet lithography, electron beam lithography, nanoimprint lithography, and nanosphere lithography (NSL), to name just a few, of which all have their own advantages and drawbacks [4–8]. NSL, more broadly natural lithography or colloidal lithography, has gained popularity as an inexpensive method for rapidly preparing nanoscale features. It features a high-throughput, in-parallel process applicable to a wide range of substrate materials, whereas the

*Correspondence: amorfa@zedat.fu-berlin.de, giersig@physik.fu-berlin.de

other previously mentioned techniques are often limited by their fabrication costs and the in-series nature of the processes, which limits the patternable area, and often need a prepatterned structure.

This technique exploits the periodic nature of a hexagonally close-packed (hcp) monolayer of nanometer- to micrometer-sized polystyrene spheres (PSSs) as a lithographic mask for physical and/or electrochemical material deposition, wet and dry etching processes, and any possible combination thereof [9–13]. Such hcp monolayers of PSSs can be created by dip-coating, electrophoretic deposition, spin-coating, and interface assembly techniques [13]. Additionally, plasma etching can be used to modify the ordered array of PSSs by reducing the polystyrene particles' size without altering the particles' location [14]. These modified or unmodified periodic particle arrays can be further used as templates for the fabrication of advanced functional materials with size-dependent optical, plasmonic, photonic, magnetic, and bionic properties [15–21], but also for the patterning of catalytically active materials as seeding points for subsequent catalytic etching or growth processes such as the growth of multiwalled carbon nanotubes (MWCNTs) by plasma enhanced chemical vapor deposition (PECVD) [22,23]

Until now, NSL has been mostly limited to academic laboratories where fabricating periodic nanostructures on planar surfaces in small quantities is desirable, although one benefit of NSL is its large area of applicability to vastly different material surfaces. Here, the roughness of the surfaces determines the degree of successful ordering of PSSs as well as the deposition of material used to fabricate functional nanostructures. In this work we illustrate the fabrication of different functional surfaces using NSL in combination with oxygen plasma etching, physical vapor deposition of metals and metal oxides, and PECVD of MWCNTs as well as their structural characterization. We discuss the influence of the substrate surface roughness on the ordering of the NSL template and on the deposition of materials. Finally, we demonstrate 10-μm rough metallic implant surfaces functionalized with periodically ordered pyramidal-shaped bulges or cylindrical cavities from NSL masks.

2. Materials and methods

2.1. Nanosphere lithography mask preparation

For the preparation of NSL masks, PSSs of uniform sizes in aqueous dispersion with a concentration of 5% by weight, purchased from Microparticles GmbH Berlin, were used. The solution was further diluted, with a ratio of 1:1, into an ethanol solution containing 1% styrene and 0.1% sulfuric acid. A custom-modified Pasteur pipette with a curved tip was used to apply the solution onto a water–air interface (18 MΩ Milli-Q water) in a petri dish where the polystyrene particles self-assembled into a hexagonally ordered array. In this work we used polished and textured n-type silicon (<100>, 0.007–0.008 Ωcm resistance, purchased from Li Jing Ke Ji), sapphire (purchased from CrysTec GmbH), and metallic medical implant disk (titanium alloy TiAl6V4 with a surface roughness of 10 μm, provided by Peter Brehm GmbH) surfaces, cleaned in acetone and then ethanol and then pure water with the aid of an ultrasonic bath for 15 min for each solvent. The silicon and sapphire surfaces were additionally treated with a subsequent piranha etch solution, which was prepared by adding concentrated sulfuric acid (96%) to concentrated hydrogen peroxide (35%) at a ratio of 3:1 for 1 h to render them hydrophilic, followed by a pure water rinse.

2.2. Dry (plasma) and wet etching

Modification of the NSL mask can be achieved by oxygen plasma treatment. Here, a Plasma Technology MiniFlecto system was used to dry etch the PSS array in an RF-plasma containing a gas mixture of argon and

oxygen. The system operates in the KHz regime at a power of 64 W. The plasma etching process is highly sensitive to several parameters such as etching duration, total gas flow rate, chamber temperature, and substrate material [14]. The decrease in PSS size can be easily controlled over the etching duration for a constant total gas flow rate and a constant chamber temperature, which were set at 3 sccm and 30–34 $^\circ$C, respectively [14]. A stabilization time of 1000 s for the gas flows was used to obtain a reproducible plasma atmosphere. The flow rates were set to 1 sccm of argon and 2 sccm of oxygen, such that the operational pressure range was between 0.1 mbar and 0.2 mbar with a chamber base pressure of 0.06 mbar.

Texturing of <100> oriented polished silicon wafers can be achieved through anisotropic chemical wet etching [24]. Here, the etching duration, etching rate, temperature, components of the solution, and its concentration determine the characteristics of the etching [24]. Applying a dilute NaOH solution containing isopropyl alcohol and deionized water onto a Si(100) surface generates pyramidal surface texturing [24]. Typically, the Si(100) surface is immersed into an aqueous solution containing 2 wt.% NaOH and 6 wt.% isopropyl alcohol at 80 $^\circ$C for 25 min. In the presented case, pyramidal surface texturing with pyramids that are typically 3 μm in height and 3 μm wide at the base were prepared.

2.3. Material deposition, mask lift off, and sample characterization

Material deposition through the mask of nickel, titanium, and silicon dioxide was performed in a custom built e-beam evaporation chamber at a deposition rate of 0.3 nm/s. The NSL mask was subsequently removed chemically by emerging the system consecutively into toluene, acetone, ethanol, and pure water in an ultrasonic bath for 15 min each in order to dissolve the PSSs and clean the surface of residual polymer residue.

MWCNTs are grown in a DC-PECVD system [25]. The custom-built PECVD chamber has a sample stage consisting of a molybdenum disk anode, which is supported by a Boralectric heating element in a tantalum heating shield, and the entire system is located in a bell jar. A Kepco BHK 2000-0.1 M DC-power supply is used to light the glow discharge plasma between the disk anode and a molybdenum rod cathode, which is spaced 1 cm above the anode. The heating element is powered by a Tectra HC 3500 Heater Controller. Two Omega FMA 5400/550 mass flow controllers are used to introduce the precursors controllably in respect to precursor ratio and total flow rate. A rotary pump is used to evacuate the system and a Pirani gauge is used to monitor the total pressure. The 0.7-μm-tall MWCNTs were grown from 60-nm-thick triangular nickel islands deposited through a NSL mask prepared from 784-nm PSSs on a silicon wafer previously coated with a 100-nm-thick titanium buffer layer for 30 min. A plasma power of 17 W, a stage temperature of 700 $^\circ$C, and a chamber pressure of 4 mbar, achieved with 40 sccm C_2H_2 and 160 sccm NH_3 mass flow, respectively, were used. The 1.3-μm-tall MWCNTs were grown from 30-nm-thick triangular nickel islands deposited through a NSL mask using 471-nm PSSs on a silicon wafer coated with a 100-nm-thick titanium buffer layer for 20 min. Here, a plasma power of 36 W, a stage temperature of 800 $^\circ$C, and a chamber pressure of 5.5 mbar, achieved with 30 sccm C_2H_2 and 180 sccm NH_3 mass flow, respectively, were used. The structural characterization of the modified and nonmodified NSL masks as well as of the different nanostructured surfaces was performed on either a Hitachi 8030 or a Carl Zeiss LEO GEMINI 1530 scanning electron microscope (SEM).

3. Results and discussion

A hexagonally close-packed monolayer of monodisperse spherical colloidal particles such as PSSs is the basis from which most NSL techniques originate. These monolayers can be self-assembled using the interface assembly technique amongst other techniques and are subsequently used as NSL masks [13]. For this purpose, an aqueous

solution of monodisperse PSSs of uniform size is applied through a Pasteur pipette with curved tip onto a water–air interface to form a monolayer (Figure 1A) until the entire surface is loosely covered (Figure 1B). PSSs with a diameter of 784 nm, which show strong diffraction colors in the visible range and that visually demonstrate the crystal domain orientations with different colors, were used for Figure 1. An individual domain size can be increased significantly to more than 25 cm^2 (Figure 1C) by applying oscillatory motions to the water–air interface. The green encircled region in Figure 1C shows a crystal area with multiple small domains, whereas the black encircled region in Figure 1C shows one large uniform crystal domain. After an adequately large area is produced, the support substrates for the NSL mask are immersed beneath the crystal, which remains at the water–air interface, and finally the water is removed by first pumping and subsequently water evaporation until the crystal is dry and sits on the substrate (Figure 1D). In Figure 1D several glass, silicon, and metal samples onto which the hcp monolayer of PSSs is deposited are shown in the red encircled area.

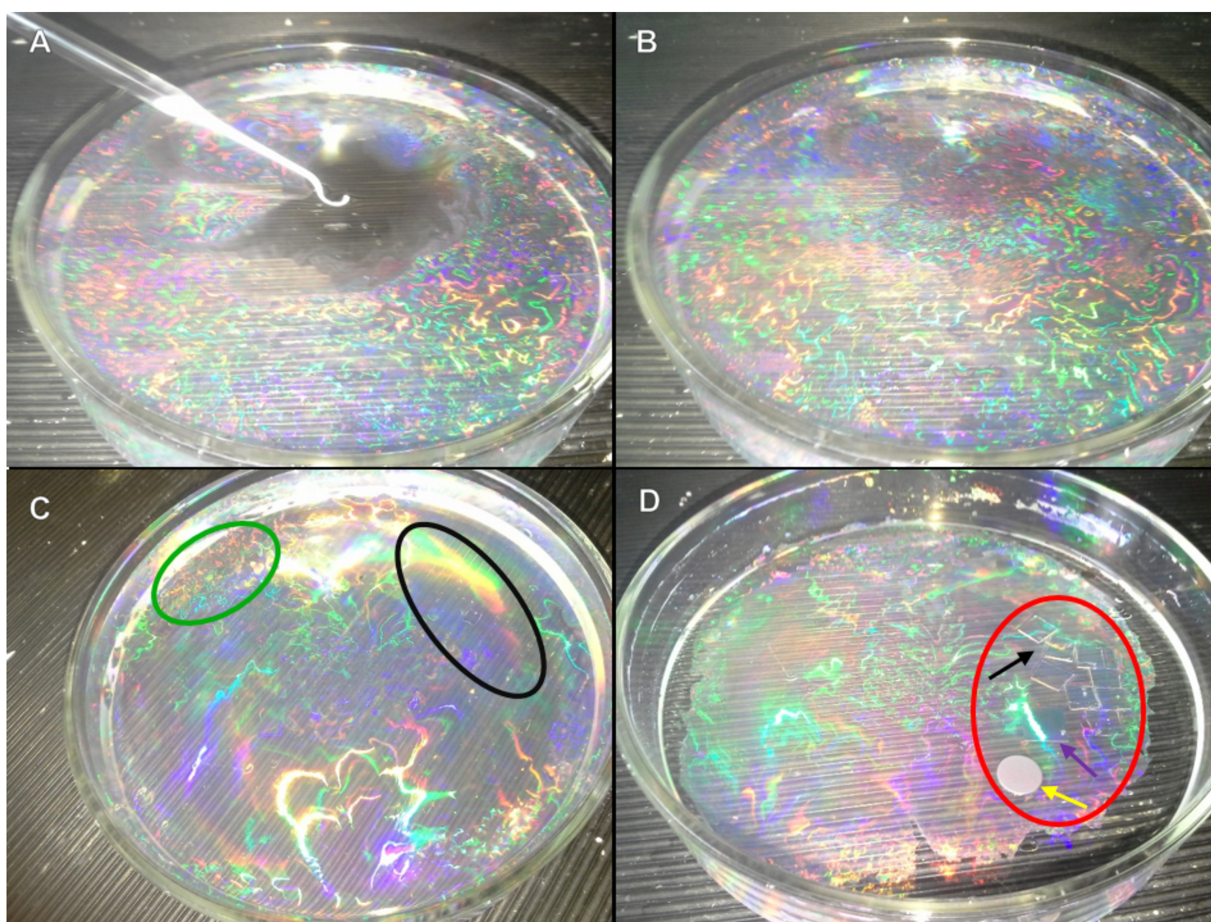

Figure 1. Preparation of a nanosphere lithography mask using the interface assembly technique. **(A)** An aqueous solution containing monodisperse polystyrene particles with diameter of 784 nm is applied to a water–air interface through a Pasteur pipette with curved tip in a petri dish. **(B)** The loosely covered surface shows strong diffraction colors that visually demonstrate the crystal domain orientations with different colors. **(C)** Individual crystal domains can be increased significantly (black encircled) by applying oscillatory motions to the water surface in contrast to the polycrystalline region (green encircled). **(D)** Different substrates (black arrow pointing towards float glass, purple arrow pointing towards Si, and yellow arrow pointing towards an orthopedic metal implant disk) are positioned below the crystal (encircled in red) previous to the removal of water to deposit the crystal onto the substrates.

Figures 2A–2H present SEM micrographs of nanostructured surfaces employing NSL. An SEM micrograph of such an hcp monolayer of PSSs of diameter 756 nm is demonstrated in Figure 2A. It is immediately clear that on a nanoscale, self-assembly produces very ordered arrays of spheres. This structure is then used as a mask during physical material deposition for controlled nanostructure fabrication. After the removal of the PSSs with an appropriate solvent, typically toluene for PSSs, only the material that is deposited through the triangular vacancies in between the individual PSSs remains. Thus, a hexagonal array of quasitriangular islands remains, with an exemplary sample shown in Figure 2C for PSSs with a diameter of 471 nm and 20 nm of deposited gold. Peng et al. showed that when produced from plasmon active material such as gold or silver, such arrays show a controllable electromagnetic response that can be tuned via the size of the triangular nanoislands [16]. To enable the removal of the NSL mask after the deposition, the maximum material deposition thickness is limited to half the PSS height (which for unaltered spheres is the initial sphere radius) [14]. Additionally, the triangular vacancy between 3 individual PSSs is reduced in size as material is deposited along the top and sides of the spheres [26]. Hence, the shape of the deposited nanoislands resembles not the shape of a triangular prism but that of a triangular pyramid. This situation is illustrated by an SEM micrograph taken at a 45° angle in Figure 2D for a sample made from PSSs with a diameter of 1.74 μm and 600 nm of deposited silicon dioxide.

The nanopatterns produced via NSL can be further used for the growth of periodically ordered and perpendicularly aligned MWCNTs through the deposition of catalytically active materials through the NSL mask und subsequent MWCNT growth by PECVD [22,25]. The MWCNT growth process is based on a vapor-liquid-solid process where a liquid catalyst, in this case molten nickel, catalyzes the growth of a solid product, the carbon nanotube, from gaseous precursors. The gaseous precursors, acetylene and ammonia gas, are decomposed at high temperatures and with the aid of an electrical glow gas discharge. Liquid nickel droplets (from the triangular nanoislands) at high temperatures $>650\ ^\circ$C act as catalytic seeds for MWCNT growth, and the initial location of the triangles defines the positions of the individual MWCNTs [25]. The bombardment of nitrogen-rich species onto the sample surfaces in the DC-plasma introduces a highly directional etching effect that results in perpendicular MWCNT alignment in a tip-growth mechanism. The MWCNTs thus grow between the substrate surface and the nickel catalyst droplets, which are continuously being ‘lifted up’ by the increasing height of the MWCNTs. Essentially, the ion bombardment etches away all deposited carbon that is deposited on the surface except for the MWCNT that is located directly beneath the nickel droplet, which acts as a protective helmet [25]. The length of the MWCNTs can be controlled by varying the growth time in the PECVD process. Typical SEM micrographs captured at a 45° angle of short (0.7 μm) and long (1.3 μm) MWCNTs grown from NSL patterned nickel catalyst arrays are shown in Figures 2E and 2F, respectively.

The diversity of nanostructures that can be fabricated using the NSL can be broadened with additional modification of the NSL mask. The PSSs can be shrunk in size without displacing the individual PSSs by exposing them to an oxygenated plasma [14]. An SEM micrograph of such a modified NSL mask is shown in Figure 2B, where the unmodified NSL mask from Figure 2A was exposed to an oxygenated RF-plasma for 400 s, resulting in reduced polystyrene particles with a diameter of 674 nm. After physical material deposition onto such a modified NSL mask and subsequent removal of the PSSs, a thin film, with a hexagonally ordered array of round perforations on the nano- or microscale depending on initial sphere size, is obtained. Thereby, thin perforated metal films can be fabricated, which were investigated as transparent electrodes for photovoltaic applications due to their partial transparency and conductivity by Morfa et al. and which were used to fabricate an enhanced broad-band extraordinary optical transmission window on strongly polarizable substrates by Sun et al. [14,21]. Such a thin perforated metal film (50-nm gold plus 3-nm titanium adhesive layer on sapphire)

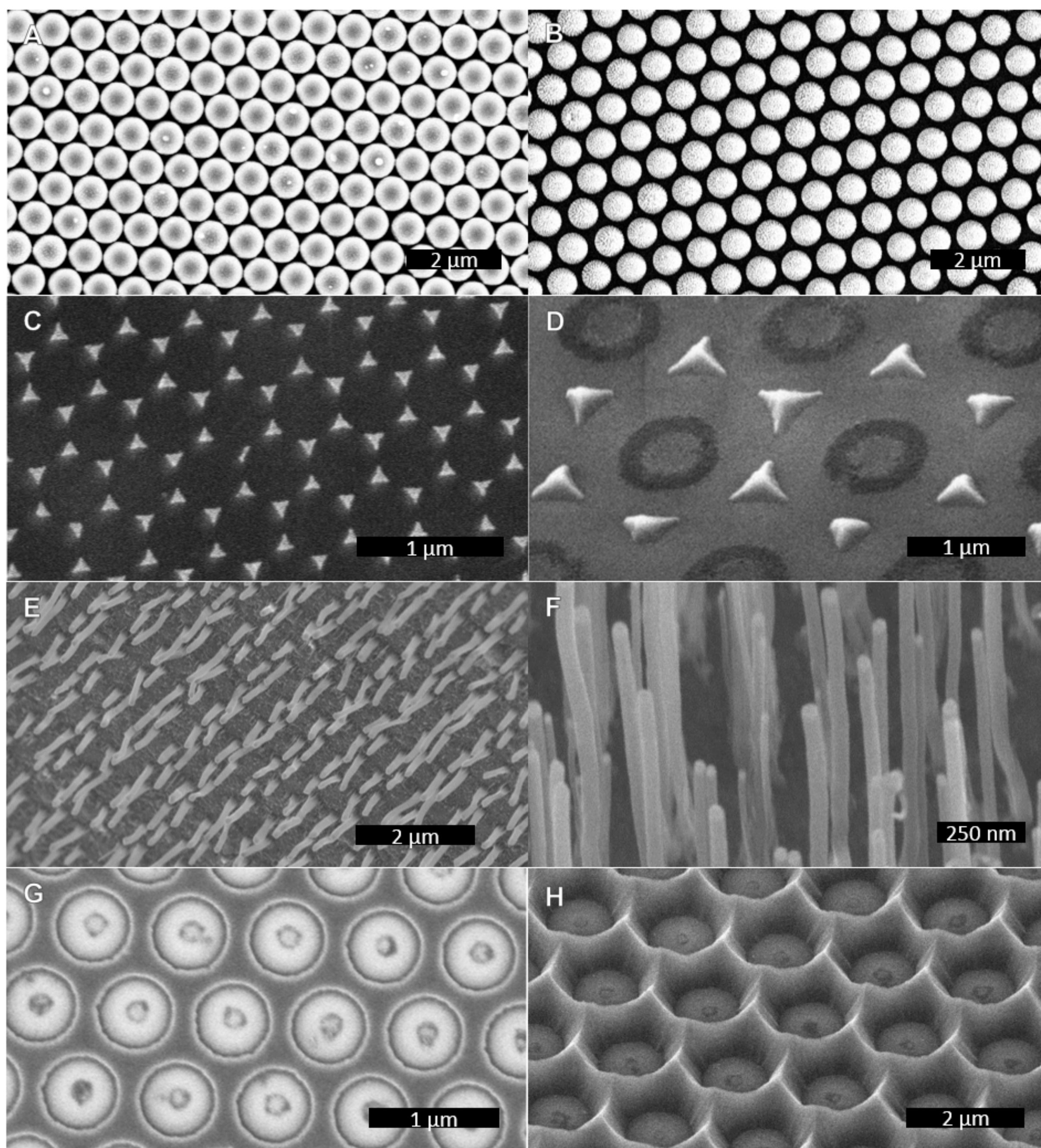

Figure 2. SEM gallery of nanostructured surfaces employing nanosphere lithography. **(A)** Monolayer of hcp polystyrene spheres with diameter of 756 nm. In **(B)** these are shrunk to 674 nm by plasma etching. Nanometer-sized arrays of 20-nm-thick triangular gold islands from 471-nm particles **(C)**, 600-nm-high pyramidal SiO_2 islands at a 45° angle from 1.74-μm particles **(D)**, 0.7tμm-tall MWCNTs from 784-nm particles **(E)**, 1.3-μm-tall MWCNTs from 471-nm particles **(F)**, perforated thin (50-nm) gold film from 756-nm particles with 568-nm holes **(G)**, and 600-nm-deep SiO_2 microcavities with 1.15-μm inner diameter at a 45° angle from 1.74-μm particles **(H)**.

with 568-nm perforations and a pitch of 756 nm is shown in Figure 2G. Additionally, this technique can be used to fabricate ceramic microcavities that may find applications as bioreactors [27,28]. An exemplary SEM

micrograph of such SiO_2 microcavities of 600 nm in depth, 1.15 μm inner diameter, and 1.74 μm pitch taken at an angle of 45° is shown in Figure 2H.

As Figure 2 demonstrates, on flat or polished surfaces on the laboratory scale, NSL is an attractive technique for the fabrication of diverse nanostructured surfaces. However, many industrially relevant objects and device surfaces do not have a flat surface (on the nano- to submicron scale). For nonflat surfaces, the ratio between the surface roughness and the utilized PSS size determines if the NSL technique can be employed to fabricate highly ordered 2-dimensional arrays of nanostructures. There are no limitations if the PSS size is very large in comparison to the surface roughness (infinite for perfectly flat surfaces) as the PSSs smoothly cover the roughness. However, the roughness breaks the hcp packing of the NSL mask for surface roughnesses similar to the PSS size. To demonstrate this situation, we prepared an NSL mask consisting of 1.74-μm PSSs onto pyramidal textured silicon surfaces with pyramids that are typically 3 μm in height and 3 μm wide at the base. The corresponding SEM micrographs are shown in Figure 3A from the top and Figure 3B from a 45° angle to illustrate the result. The hcp ordering of the NSL mask is completely broken and the majority of the PSSs sit on top of each other in the valleys of the textured silicon surface. In contrast, when the surface roughness is significantly larger than the PSS size, the NSL mask is deposited on the flat surfaces of the larger-scale roughness. This situation is demonstrated with 471-nm PSSs on the previously described

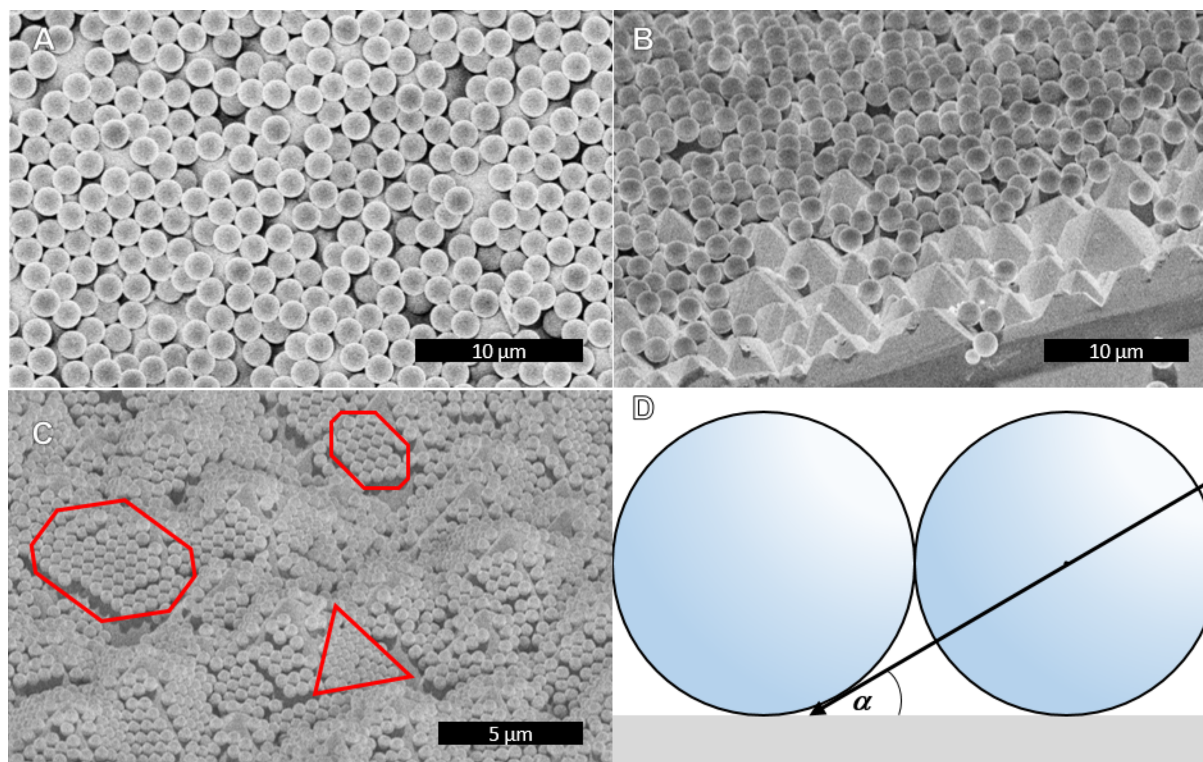

Figure 3. Application of nanosphere lithography to textured surfaces. **(A)** Top view and **(B)** 45° angle view of 1.74-μm particles on a pyramidal textured silicon surface with pyramids that are typically 3 μm in height and 3 μm wide at base. The roughness does not allow hcp ordering of the polystyrene particles. **(C)** A 45° angle view of 471-nm particles on the pyramidal textured silicon surface. The hcp monolayer polystyrene breaks up into small fractions, which sit on the inclinations of the surface (encircled in red). **(D)** No material is deposited for material trajectory angles $\alpha < 35^\circ$ during material deposition so that no material can be deposited on inclinations with a slope $\beta > 55^\circ$.

pyramidal textured silicon surface in Figure 3C. Clearly, the large-area hcp monolayer of PSSs separated into many small, spaced-out areas of hcp PSSs (encircled in red) as the surface area of the textured surface is much larger than the area of the NSL mask. Additionally, the slope of the inclined surface introduces a shadow effect during physical material deposition techniques that may greatly influence the outcome. From the geometric perspective, material deposition through the triangular vacancies between 3 PSSs is only possible for inclination angles $\beta < 55°$ ($\beta = 90° - \alpha$) considering a straight trajectory of deposited material (Figure 3D). However, it was shown that this shadow effect can be exploited to fabricate further sophisticated nanostructures such as nanowires, nanorings, and nano split-ring resonators [9,10].

For biological samples, some nanostructured surfaces have been shown to influence the adhesion and activity of osteoblasts, whereas others were shown to inhibit the bacterial adhesion and biofilm formation of *Escherichia coli* and *Staphylococcus aureus* [29,30]. Therefore, a rational nanostructure design of medically relevant surfaces has many potential applications in life sciences [30]. For this purpose, the broad range of different nanostructures with well-defined morphologies that can be fabricated from vastly different materials using NSL are attractive for their application on medical devices where customized surface properties are desired. Here, we demonstrate the successful application of NSL onto commonly used rough ($R_z = 10$ μm) titanium alloy orthopedic implant surfaces, as shown in Figure 4. Two representative structures, in particular pyramidal SiO_2 islands (350 nm in height, 784 nm pitch) and SiO_2 microcavities (250 nm in depth, 784 nm pitch, 630 nm inner diameter), are shown in Figures 4A and 4B, respectively. From the SEM micrographs it is clear that the rough surface is textured with the intended nanostructures. These and similar structures can be fabricated from SiO_2 and also from many different other solid materials. Consequently, NSL can be used to fabricate vastly different nanostructured surfaces on medical devices where a nanostructured morphology of different materials is needed to customize them for individual application.

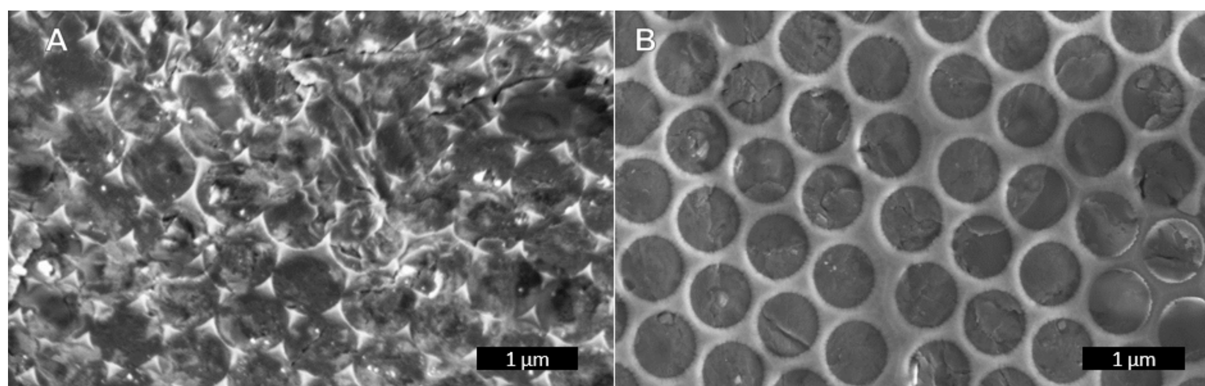

Figure 4. Application of nanosphere lithography to rough orthopedic surfaces: 350-nm-high pyramidal SiO_2 islands from 784-nm particles **(A)** and 250-nm-deep SiO_2 microcavities with 630-nm inner diameter from 784-nm particles plasma etched for 400 s **(B)** on 10-μm rough orthopedic titanium alloy implants.

In conclusion, we have demonstrated how to use the NSL technique to fabricate 2-dimensional arrays of sophisticated nanostructures such as triangular and pyramidal nanoislands, periodically perforated films, microcavities, and multiwalled carbon nanotube arrays. We discussed the effect of the support surface roughness in comparison to the PSS size and showed that the roughness needs to be very small or very large with regard to the sphere size. Finally, we demonstrated that NSL is suitable to nanotexture the surface of rough medical implant surfaces with different nanostructures.

Acknowledgments

The authors wish to acknowledge Dr K Ellmer of HZB for assistance with the physical vapor deposition. AJM acknowledges AvH Stiftung for financial support. MG acknowledges financial support by the National Science Centre allocated on the basis of the decision number DEC-2013/06/A/ST4/00373. EMA acknowledges financial support by the European Union under the project CosmoPHOS with the number 310337.

References

[1] Neinhuis, C.; Barthlott, W. *Ann. Bot.* **1997**, *79*, 667–677.

[2] Gao, X.; Yan, X.; Yao, X.; Xu, L.; Zhang, K.; Zhang, J.; Yang, B.; Jiang, L. *Adv. Mater.* **2007**, *19*, 2213–2217.

[3] Gates, B. D.; Xu, Q.; Stewart, M.; Ryan, D.; Willson, C. G.; Whitesides, G. M. *Chem. Rev.* **2005**, *105*, 1171–1196.

[4] Chen, Y.; Pépin, A. *Electrophoresis* **2001**, *22*, 187–207.

[5] Deckman, H. W.; Dunsmuir, J. H. *Appl. Phys. Lett.* **1982**, *41*, 377–379.

[6] Denkov, N. D.; Velev, O. D.; Kralchevski, P. A.; Ivanov, I. B.; Yoshimura, H.; Nagayama, K. *Langmuir* **1992**, *8*, 3183–3190.

[7] Giersig, M.; Mulvaney, P. *Langmuir* **1993**, *9*, 3408–3413.

[8] Hulteen, J. C.; Van Duyne, R. P. *J. Vac. Sci. Technol. A* **1995**, *13*, 1553–1558.

[9] Kosiorek, A.; Kandulski, W.; Chudzinski, P.; Kempa, K.; Giersig, M. *Nano Lett.* **2004**, *4*, 1359–1363.

[10] Kosiorek, A.; Kandulski, W.; Glaczynska, H.; Giersig, M. *Small* **2005**, *1*, 439–444.

[11] Haginoya, C.; Ishibashi, M.; Koike, K. *Appl. Phys. Lett.* **1997**, *71*, 2934–2936.

[12] Schmitt, S. W.; Schechtel, F.; Amkreutz, D.; Bashouti, M.; Srivastava, S. K.; Hoffmann, B.; Dieker, C.; Spiecker, E.; Rech, B.; Christiansen, S. H. *Nano Lett.* **2012**, *12*, 4050–4054.

[13] Yang, S. M.; Jang, S. G.; Choi, D. G.; Kim, S.; Yu, H. K. *Small* **2006**, *2*, 458–475.

[14] Akinoglu, E. M.; Morfa, A. J.; Giersig, M. *Langmuir* **2014**, *30*, 12354–12361.

[15] Jensen, T. R.; Malinsky, M. D.; Haynes, C. L.; Van Duyne, R. P. *J. Phys. Chem. B* **2000**, *104*, 10549–10556.

[16] Peng, Y.; Marcoux, C.; Patoka, P.; Hilgendorff, M.; Giersig, M.; Kempa, K. *Appl. Phys. Lett.* **2010**, *96*, 133104.

[17] Ctistis, G.; Papaioannou, E.; Patoka, P.; Gutek, J.; Fumagalli, P.; Giersig, M. *Nano Lett.* **2009**, *9*, 1–6.

[18] Akinoglu, E. M.; Sun, T.; Gao, J.; Giersig, M.; Ren, Z.; Kempa, K. *Appl. Phys. Lett.* **2013**, *103*, 171106.

[19] Wood, M. A. *J. R. Soc. Interface* **2007**, *4*, 1–17.

[20] López-García, M.; Galisteo-López, J. F.; Blanco, Á; López, C.; García-Martín, A. *Adv. Funct. Mater.* **2010**, *20*, 4338–4343.

[21] Sun, T.; Akinoglu, E. M.; Guo, C.; Paudel, T.; Gao, J.; Wang, Y.; Giersig, M.; Ren, Z.; Kempa, K. *Appl. Phys. Lett.* **2013**, *102*, 101114.

[22] Huang, Z. P.; Carnahan, D. L.; Rybczynski, J.; Giersig, M.; Sennett, M.; Wang, D. Z.; Wen, J. G.; Kempa, K.; Ren, Z. F. *Appl. Phys. Lett.* **2003**, *82*, 460.

[23] Wang, H. P.; Lai, K. Y.; Lin, Y. R.; Lin, C. A.; He, J. H. *Langmuir* **2010**, *26*, 12855–12858.

[24] Iftiquar, S. M.; Lee, Y.; Ju, M.; Balaji, N.; Dhungel, S. K.; Yi, J. In *Photodiodes - From Fundamentals to Applications*; Yun, I., Ed. InTech: Rijeka, Croatia, 2012, pp. 105–132.

[25] Ren, Z.; Lan, Y.; Wang, Y. *Aligned Carbon Nanotubes*; Springer: Berlin, Germany, 2013.

[26] Ye, S.; Routzahn, A. L.; Carroll, R. L. *Langmuir* **2011**, *27*, 13806–13812.

[27] Grayson, W. L.; Martens, T. P.; Eng, G. M.; Radisic, M.; Vunjak-Novakovic, G. *Sem. Cell Dev. Biol.* **2009**, *20*, 665–673.

[28] Retterer, S. T.; Siuti, P.; Choi, C. K.; Thomas, D. K.; Doktycz, M. J. *Lab Chip* **2010**, *10*, 1174–1181.

[29] Price, R. L.; Haberstroh, K. M.; Webster, T. J. *Med. Biol. Eng. Comput.* **2003**, *41*, 372–375.

[30] Singh, A. V.; Vyas, V.; Patil, R.; Sharma, V.; Scopelliti, P. E.; Bongiorno, G.; Podestà, A.; Lenardi, C.; Gade, W. N.; Milani, P. *PLoS ONE* **2011**, *6*, e25029.